



Article scientifique

Article

2018

Accepted version

Open Access

This is an author manuscript post-peer-reviewing (accepted version) of the original publication. The layout of the published version may differ .

Nanocrystals of a potent p38 MAPK inhibitor embedded in microparticles: Therapeutic effects in inflammatory and mechanistic murine models of osteoarthritis

Maudens, Pierre Marc Xavier; Seemayer, Christian Alexander; Pfefferlé, François; Jordan, Olivier;
Allémann, Eric

How to cite

MAUDENS, Pierre Marc Xavier et al. Nanocrystals of a potent p38 MAPK inhibitor embedded in microparticles: Therapeutic effects in inflammatory and mechanistic murine models of osteoarthritis. In: Journal of Controlled Release, 2018, vol. 276, p. 102–112. doi: 10.1016/j.jconrel.2018.03.007

This publication URL: <https://archive-ouverte.unige.ch/unige:141549>

Publication DOI: [10.1016/j.jconrel.2018.03.007](https://doi.org/10.1016/j.jconrel.2018.03.007)

Nanocrystals of a potent p38 MAPK inhibitor embedded in microparticles: therapeutic effects in inflammatory and mechanistic murine models of osteoarthritis

5 *Pierre Maudens¹, Christian Alexander Seemayer², François Pfefferlé³, Olivier
Jordan¹ and Eric Allémann¹*

¹School of Pharmaceutical Sciences, University of Geneva, University of Lausanne, CH-1211
Geneva 4, Switzerland

10 ²Department of Clinical Science, Idorsia Pharmaceuticals Ltd., CH-4123 Allschwil,
Switzerland

³Debiopharm Research and Manufacturing, CH-1920 Martigny, Switzerland

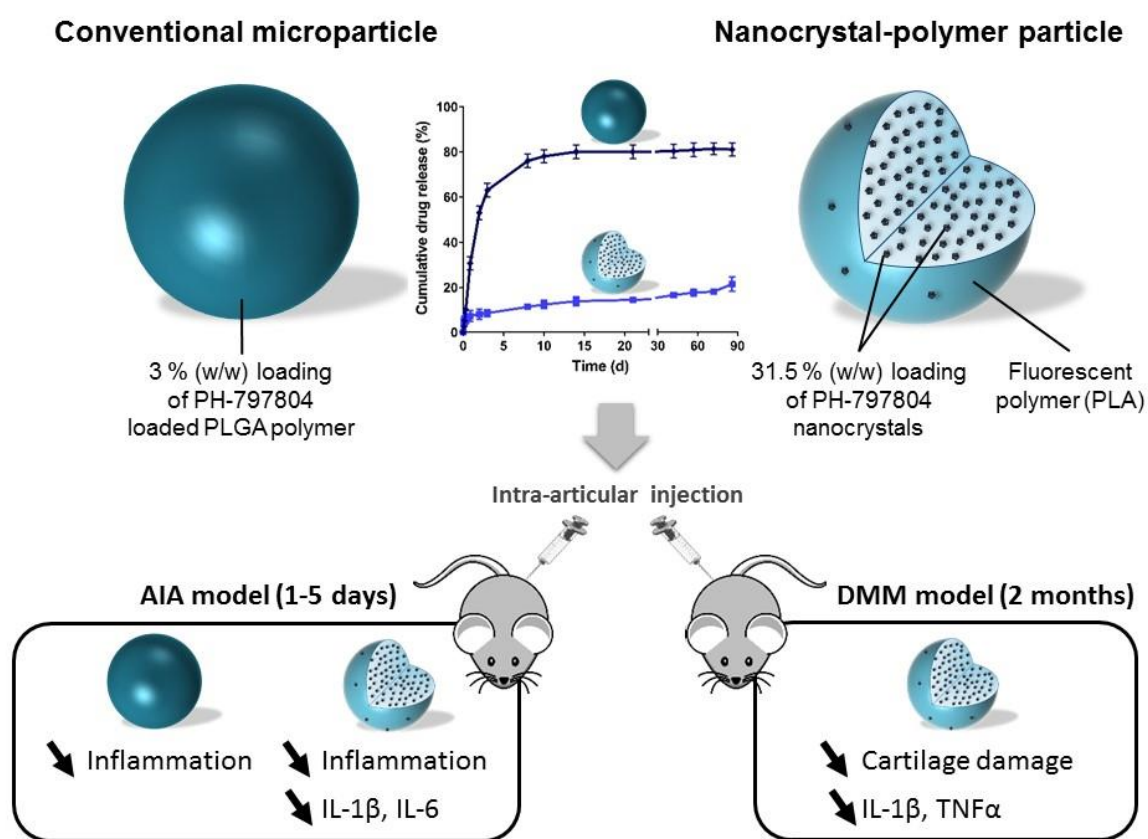
15

Abstract

This study aimed to formulate nanocrystal-polymer particles containing the potent p38 α / β MAPK inhibitor PH-797804 (PH-NPPs) and to test their extended-release properties over months in comparison to those of conventional PH microparticles for the intra-articular treatment of inflammatory and mechanistic murine models mirroring aspects of human osteoarthritis (OA). The steps of the study were (i) to formulate PH nanocrystals (wet milling), (ii) to encapsulate a high payload of PH nanocrystals in fluorescent particles (spray drying), (iii) to assess *in vitro* drug release, (iv) to evaluate PH-NPP toxicity to human OA synoviocytes (MTT test), (v) to investigate the *in vivo* bioactivity of the particles in mice in an inflammatory antigen-induced arthritis (AIA) model (using histology and RT-qPCR) and (vi) to investigate the *in vivo* bioactivity of the particles in the OA model obtained by mechanistic surgical destabilization of the medial meniscus (DMM) (using histology, micro-CT, and multiplex ELISA). The PH nanocrystals stabilized with vitamin E TPGS had a monomodal size distribution. The PH-NPPs had a mean diameter of 14.2 μ m and drug loading of ~31.5 % (w/w), and ~20 % of the PH was released over 3 months. The NPPs did not exhibit toxicity to cultured human OA synoviocytes at 100 \times IC₅₀. Finally, *in vivo* studies showed good retention of PH-NPPs in the joint and adjacent tissues for up to 2 months, and the PH-NPPs exhibited good functional relevance by significantly reducing inflammation and joint destruction and by inhibiting several biomarkers (e.g., IL-1 β). In conclusion, local treatment with PH-NPPs, used as an

extended-release drug delivery system, ameliorated inflammation and joint degradation in two distinct mouse models, indicating treatment potential for human OA.

Graphical abstract



5

Keywords

PH-797804; biodegradable microparticles; nanocrystals; inflammatory and mechanistic mouse models; osteoarthritis; intra-articular administration; extended

drug delivery; p38 α / β MAPK inhibitor

Abbreviations

^{99m}Tc: technetium-99m; AIA: antigen-induced arthritis; DMM: destabilization of the medial meniscus; DSC: differential scanning calorimetry; DXM: dexamethasone 21-acetate; ELISA: enzyme-linked immunosorbent assay; IA: intra-articular; ID: intradermal; IL-17: interleukin-17; IL-1 β : interleukin-1 β ; IL-6: interleukin-6; mBSA: methylated bovine serum albumin; micro-CT: micro-computed tomography; MPs: microparticles; MTT: 3-(4,5-dimethylthiazol-2-yl)-2,5-diphenyltetrazolium bromide; NPPs: nanocrystal-polymer particles; OA: osteoarthritis; OARSI: Osteoarthritis Research Society International; PH: PH-797804; PLA: poly(lactic acid); PLGA: poly(lactic-co-glycolic acid); RT-qPCR: quantitative reverse transcription polymerase chain reaction; SOFG: safranin-O/fast green; TNF α : tumor necrosis factor- α ; TPGS: d- α -tocopheryl polyethylene glycol 1000 succinate; UHPLC: ultra-high-performance liquid chromatography; VEGF: vascular endothelial growth factor.

15

Acknowledgments

The authors thank the following people for their assistance: P. Garrouste and L. Tamarcaz for the spray drying; C. Gabay for his participation and help for the *in vitro* trials, G. Palmer and D. Talabot for RT-qPCR measurements; L. Neff for the *in*

vivo experiments; and D. Guillarme and V. Desfontaine for the UHPLC-MS/MS *triple* quadrupole method development.

Introduction

Fifteen percent of the global population over 60 years of age suffers from
5 osteoarthritis (OA) [1], which is the most common joint disease [2]. In OA, the
cartilage breaks down and eventually wears away, causing pain (inflammation),
swelling and reduced joint mobility. As cartilage degenerates over time, the bone may
also be affected and react by the development of osteophytes. Fragments of bone or
cartilage may chip off and float around in the joint. An inflammatory process occurs
10 in the body, and pro-inflammatory cytokines [3] and enzymes are released that further
damage the cartilage. Pain occurs during or after articular activity and fades with rest.
Most of the available OA treatments are oral and neither provide adequate pain relief
nor slow down or stop the evolution of the underlying disease. Because of the
localized nature of OA, which generally affects only one or two joints, the intra-
15 articular (IA) injection of a drug delivery system is an attractive treatment approach
that would allow high local drug concentrations while limiting systemic exposure and
associated side effects [4, 5].

PH-797804 (PH) is a potent and selective ATP-competitive p38 α / β mitogen-
activated protein kinase (MAPK) inhibitor (the IC₅₀ values are 26 and 102 nM for α
20 and β , respectively) [6-8]. PH blocks RANKL- and M-CSF-induced osteoclast
formation in primary rat bone marrow cells [6]. PH inhibits lipopolysaccharide-induced

IL-1 β and TNF α production in primary human monocytes in a concentration-dependent manner and inhibits the increase of inflammatory mediators in healthy patients [9]. Signaling through p38 α/β MAPK then reduces inflammatory effects, which play an important role in OA and rheumatoid arthritis (RA) [10-12]. PH has reached phase II trials using oral administration once daily for four weeks in patients with RA (NCT00620685) but failed to demonstrate clinical efficacy [13]. Indeed, PH bioactivity was observed in RA patients, but the effect faded after two weeks. The results suggest that PH may not provide meaningful and sustained suppression of inflammation when administered orally. Another phase II clinical trial (NCT01102660) focusing on patients with knee OA is currently in progress and compares the pain relief resulting from the oral administration of PH *versus* naproxen. In this context, for effective OA treatment, PH would require a delivery system with sustained/extended release lasting for months.

Microparticles (MPs) composed of biodegradable and biocompatible polymers, such as poly(lactic-co-glycolic acid) (PLGA) or poly(lactic acid) (PLA), have been widely used as matrices for drug delivery to achieve controlled drug release [14, 15]. They have been approved for a variety of clinical applications by the Food and Drug Administration (FDA) and European Medicines Agency (EMA). Based on a previous study by our group, particles with diameters ranging from 10 to 25 μm were retained for months in the joint and adjacent tissues of mice [16]. Recently, nanocrystals-polymer particles (NPPs) were developed that tend toward zero-order kinetics with high drug loading in polymeric microparticles, with a size that prevents

fast clearance from the joint space [17]. This innovation combines the advantages of nanocrystals and spray-dried microparticles to approach an ideal drug delivery system for IA administration.

The aim of this study was to formulate and evaluate the safety and efficacy of the PH-NPP system *in vitro* and in murine models. To this end, (i) we developed and optimized the formulation of PH nanocrystals and (ii) PH nanocrystal-loaded NPPs (PH-NPPs) containing a fluorescent polymer for *in vivo* intravital tracking. The anti-inflammatory steroid dexamethasone 21-acetate (DXM) was used as a control compound. Conventional microparticles (MPs) loaded with PH (PH-MPs) or DXM (DXM-MPs) were formulated as negative controls. All the microparticles were characterized (e.g., size, morphology, *in vitro* drug release profile). The compatibility of the particles with OA human synovial fibroblasts was investigated *in vitro*. Particles were injected into (v) an inflammatory antigen-induced arthritis (AIA) mouse model and (vi) a mechanistic surgical destabilization of the medial meniscus (DMM) mouse model. Finally, the biodistribution of the active pharmaceutical ingredients (APIs), the expression levels of OA biomarkers, and a histology score were used to confirm the bioactivity of the APIs.

Materials and methods

Formulation of API nanocrystals

PH-797804 (PH) and dexamethasone 21-acetate (DXM) were purchased from
5 Sigma-Aldrich (St. Louis, MO, USA) and Tocris (Bristol, UK), respectively. Five
milligrams of API was dissolved in 300 μ L of organic solvent (acetone for PH and
ethanol for DXM) in a 2-mL tube containing 579 mg of 0.5 mm zirconium TriplePure
M-Bio Grade beads purchased from Sigma-Aldrich (St. Louis, MO, USA).
Crystallization was performed by adding 600 μ L of distilled water as a non-solvent,
10 and the tube was left open overnight at 4 °C to allow slow evaporation of the solvent.
Then, 100 μ L of D- α -tocopherol polyethylene glycol 1,000 succinate (TPGS),
purchased from Sigma-Aldrich, was added as a stabilizer (2 % (w/v)). The crystals
were reduced in size by placing the tubes on a Vortex-Genie 2 (Scientific Industries,
Inc, Bohemia, NY, USA) fitted with a horizontal microtube holder obtained from
15 Labgene Scientific SA (Châtel-Saint-Denis, Switzerland) for 6 h at 2700 RPM. The
particle size was measured by dynamic light scattering (DLS) (Nanosizer, Malvern,
England) in triplicate. Nanocrystals were separated from supernatant at 10,000 \times g
for 15 min by using a Beckman Avanti 30 centrifuge (Beckman Coulter, Brea, CA,
USA). Finally, nanocrystals were lyophilized for 2 days and stored at 4 °C.

20

Formulation of nanocrystal-polymer particles (NPPs)

Poly(D, L-lactic acid) (PLA) (Purac®, molecular weight: 65 kDa) was provided by Corbion (Diemen, the Netherlands). Approximately 38 mg·mL⁻¹ of PLA and 1.7 mg·mL⁻¹ of PLA-Cyanine 7 (PLA-Cy7, synthesized as previously described [17]) were dissolved in organic solvent (dichloromethane for DXM-NPPs and ethyl acetate for PH-NPPs) with a magnetic stirrer. Then, drug nanocrystals were suspended in the polymer solution at a concentration of 23.4 mg·mL⁻¹ and immediately spray-dried to formulate NPPs using ProCept 4M8-TriX, protected from light by a nitrogen closed-loop recirculation unit (ProCepT Processing Equipment, Zelzate, Belgium). The following processing parameters were used: M cyclone size; 20 % pump position; small (Ø 1.6 mm) tubing size for the peristaltic pump; 80 °C temperature inlet; 0.4 m³·min⁻¹ air flow; 0.6 mm nozzle size; round spray air cap; 5 L·min⁻¹ nozzle flow; 40-50 mbar differential pressure cyclone; and 140 L·min⁻¹ air carrier flow. The NPPs were collected, dried in an oven at 37 °C under vacuum, lyophilized for 2 days and stored at 4 °C with protection from light. Blank NPPs were formulated with the same method except that the mass of nanocrystals was replaced with PLA, which was then dissolved in dichloromethane.

Formulation of MPs

MPs were prepared by an emulsion-solvent extraction method. Poly(D, L-lactide-co-glycolide) (PLGA 75:25, molecular weight: 15 kDa) was provided by Boehringer Ingelheim (Ingelheim am Rhein, Germany) (Resomer® RG 752S). Poly(vinyl alcohol) (PVAL) was a gift from Clariant GmbH (Frankfurt am Main,

Germany) (Mowiol® 4-88, hydrolysis degree 88 %, molecular weight 26 kDa). One milliliter of organic phase (ethyl acetate:ethanol (9:1)) containing 300 mg·mL⁻¹ RG 752S and 10 mg·mL⁻¹ API (PH or DXM) was emulsified with 2 mL of 2 % PVAL solution using a T25 Ultra-Turrax (IKA Werke GmbH & Co., Staufen im Breisgau, Germany) for 1 min at 13,500 RPM. Then, the emulsion was poured into 20 mL of distilled water and mechanically stirred for 4 h at room temperature and 400 RPM (Eurostar Digital, IKA Werke GmbH & Co.) The resulting MPs were separated at 280 RCF by using a Beckman Avanti 30 centrifuge (Beckman Coulter, Brea, CA, USA), washed 3 times with distilled water, freeze-dried for 2 days (EF4 Modulyo, Edwards, Switzerland) and finally stored at 4 °C. Blank MPs were formulated using the same method.

Size, morphology, encapsulation efficiency and drug loading

The size of the MPs and NPPs was determined by laser light diffraction (Mastersizer S, Malvern Instruments Ltd., Malvern, UK). Dynamic light scattering (Nanosizer, Malvern, England) was used to determine the size of the nanocrystals and the zeta potentials of the MPs and NPPs. After drying and coating with a 20-nm gold layer (Leica EM SCD 500, Leica Microsystems GmbH, Wetzlar, Germany), the morphology was determined by scanning electron microscopy (Jeol Microscope, JSM-7001TA, Tokyo, Japan) at an accelerating voltage of 5 kV. Cross sections were obtained by first embedding NPPs in an epoxy resin and then cutting them on a Leica UCT Ultramicrotome (Wetzlar, Germany) using a diamond blade. They were also

observed by scanning electron microscopy. The drug encapsulation efficiency (1) and drug loading (2) into the microparticles were determined by reversed-phase UHPLC and calculated based on the following equations:

$$\text{Encapsulation efficiency} = \frac{\text{wt Drug entrapped}}{\text{wt Theoretical drug loading}} \times 100 \quad (1)$$

5

$$\text{Drug loading} = \frac{\text{wt Drug entrapped}}{\text{wt Microparticles}} \times 100 \quad (2)$$

Ultra-high-performance liquid chromatography (UHPLC)

The APIs were quantified by reversed-phase UHPLC using a Thermo Fisher
10 Accela system and a C18 Hypersil gold column 50/2.1 with a 1.9 μm bead particle size (Thermo Fisher Scientific, Waltham, MA, USA). The mobile phase comprised 0.1 % v/v trifluoroacetic acid (TFA) in water (A) and 0.1 % v/v TFA in acetonitrile (B), and the following gradient elution sequence was applied at a flow rate of 400 $\mu\text{L}\cdot\text{min}^{-1}$:
30-95 % A (0–3 min), 95–10 % A (3-4 min), 10-30 % A (4-4.5 min) and 30 % A (4.5–
15 5 min) (retention time: 1.9 min for PH and 1.6 min for DXM). The detection limit of PH and DXM was about 1 ppm.

Residual solvent

A gas chromatograph (Agilent Technologies GC Agilent 6850) equipped with
20 a flame ionization detector, a headspace sampler (Agilent 7694 Headspace) and a DB-624 column (30 m \times 0.32 mm \times 1.8 μm) was used to determine the residual

dichloromethane and ethyl acetate in the NPPs. According to the USP 467 method and European Pharmacopoeia 9.0 (2.4.24. and 5.4.), the concentration limit of dichloromethane and ethyl acetate in pharmaceutical products is 600 and 5,000 ppm, respectively. Gas chromatography was performed at an oven temperature of 200 °C, an injector temperature of 140 °C, a detector temperature of 250 °C and a carrier flow (nitrogen) of 45 mL·min⁻¹.

Differential scanning calorimetry (DSC)

The DSC study was performed with a SEIKO SSC5200 (Seiko Instruments, Chiba, Japan). All crucibles containing 5-10 mg of lyophilized sample were first heated from 25 to 110 °C at a rate of 10 °C·min⁻¹ to erase any thermal history. Then, the oven was cooled with liquid nitrogen to -10 °C at a rate of 20 °C·min⁻¹ and finally heated from -10 to 300 °C at a rate of 5 °C·min⁻¹. The glass transition temperature (T_g) and the phase transition temperature (T_m) were determined by the DSC curve from the final heating run.

Injectability

The maximum force of a syringe filled with MPs or NPPs dispersed in PBS (maximum concentration injected *in vivo*) was determined at 20 °C using a speed of 1 mm·s⁻¹ on a TA.XTPlus Texture Analyzer (Tracomme AG, Switzerland). A 1 mL BD Micro-Fine™ 29G fixed-needle insulin syringe (later used in this study for the IA

injections into mice) was used.

***In vitro* drug release**

To determine the drug release profile from the MPs and NPPs, *in vitro* drug
5 release was conducted under sink conditions in PBS at pH 7.4 with 0.1 % sodium
dodecyl sulfate. The suspension was horizontally shaken at 80 RPM and 37 °C in a
GFL-3033 orbital shaker (Burgwedel, Germany). The solubility of PH and DXM in
PBS were 300 and 100 ppm, respectively. The drug released at each time point was
quantified by reversed-phase UHPLC. The withdrawn volume was replaced with
10 fresh PBS. All experiments were performed in triplicate.

Cell viability assay

The mitochondrial activity of OA human fibroblast-like synoviocytes (passage
8, n = 3) was assessed in contact with blank NPPs (0.002, 0.02, 0.2, 2, and 20 mg·mL⁻¹
15 (concentration injected *in vivo*)), DXM-NPPs (0.1, 1, 10 (IC₅₀), 100, and 1,000 nM
of DXM), and PH-NPPs (0.26, 2.6, 26 (IC₅₀), 260 and 2,600 nM of PH). The
permission for the study on human tissues was given by the Central Committee for
Ethics in Research of Geneva University Hospital (CER: 05-007 (05-017)). The cells
were plated at a density of 20,000 cells/well in 96-well plates. After 24 h, NPPs were
20 suspended in PBS and incubated for 24 h at 37 °C. Approximately 50 µL of 0.5 % 3-
(4,5-dimethylthiazol-2-yl)-2,5-diphenyltetrazolium bromide (MTT) solution was added
to each well, and the plates were left for 3 h. All wells were incubated for 45 min with

100 μL of DMSO, and the absorbance was measured at 570 nm (8 points per well) on a BioTeK Synergy Mx microplate reader (Winooski, VT, USA).

Adjuvant-induced arthritis (AIA) model in C57Bl/6 mice

5 *In vivo* experiments were performed in compliance with the Swiss Federal Law on the Protection of the Animals. The protocols were accepted by the Geneva Authority (GE/148/14). AIA was induced in male C57Bl/6 mice as previously described [18, 19] with minor modifications (Fig. 3a). In brief, 2 $\text{mg}\cdot\text{mL}^{-1}$ methylated bovine serum albumin (mBSA) (Sigma-Aldrich) in PBS was emulsified at 50:50 with
10 Freund's complete adjuvant (Thermo Fisher Scientific) containing 1 $\text{mg}\cdot\text{mL}^{-1}$ mycobacterium tuberculosis. This emulsion was obtained using an Ultra-Turrax T25 (IKA Werke GmbH & Co) at 13,500 RPM for 1 minute in a tube immersed in ice water. At day 0, the mice ($n = 5-7$ per group) were immunized by intradermal (ID) injection into the tail root with 100 μL of mBSA/Freund's complete adjuvant emulsion.

15 A second immunization was performed on day 7 *via* the intradermal injection of 100 μL of 2 $\text{mg}\cdot\text{mL}^{-1}$ mBSA emulsified 1:1 with Freund's incomplete adjuvant (Sigma-Aldrich). Arthritis was induced on day 21 by the intra-articular (IA) injection under a 10 \times binocular microscope of 10 μL of 10 $\text{mg}\cdot\text{mL}^{-1}$ mBSA in PBS into the medial joint cavity of the right knee. Concomitantly with the arthritis induction, MPs or
20 NPPs were injected in the same syringe. The API doses of injected PH-NPPs, DXM-NPPs, PH-MPs, and DXM-MPs corresponded to 2.5, 2.01, 5, and 0.12 $\text{mg}\cdot\text{kg}^{-1}$, respectively. The right knee was injected, as a control, with PBS. The joint

inflammation was quantified by measuring the accumulation of technetium-99m (^{99m}Tc) pertechnetate in the knee at day 22 (MINI-assay type 6-20 H gamma counter; Uehlinger-Pfiffner AG, Schöftland, Switzerland). Thus, a dose of 10 μCi ^{99m}Tc per mouse was subcutaneously (SC) injected into the posterior neck region. The
5 accumulation of the isotope was measured 30 minutes after the SC injection by external gamma counting. The acquisition time was set at 10 seconds per knee ($n = 3$), with repositioning of the mouse knee between the measurements. The ratio of ^{99m}Tc accumulation in the inflamed arthritic knee to ^{99m}Tc uptake in the contralateral control knee (left knee) was calculated. A ratio larger than 1.1 was considered a sign
10 of joint inflammation. The mice were sacrificed at day 25 and the joints further processed for histological and biological assessments (see below).

Quantitative reverse transcription polymerase chain reaction (RT-qPCR) (AIA model)

15 Knees were collected after sacrifice. The total RNA was extracted with TRIzol reagent (Thermo Fisher Scientific), purified with the RNeasy Mini Kit (Qiagen, Venlo, Netherlands), and reverse-transcribed using SuperScript II Reverse Transcriptase (Invitrogen Life Technologies, Basel, Switzerland) according to the manufacturer's instructions. The mRNA levels of genes of interest were examined by RT-qPCR using
20 the iCycler iQ Real-Time PCR Detection System (standard protocol, 40 cycles, annealing temperature 60 °C), iQ™ SYBR® Green Supermix (Bio-Rad, Hercules, CA, USA) and the following primers: interleukin-1 β (IL-1 β): forward primer 5'-

TGTGAAATGCCACCTTTTGA-3', reverse primer 5'-GTGCTCATGTCCTCATCCTG-3'; interleukin-6 (IL-6): forward primer 5'-TGAACAACGATGATGCACTTGCAGA-3', reverse primer 5'-TCTGTATCTCTCTGAAGGACTCTGGCT-3'; tumor necrosis factor- α (TNF α): forward primer 5'-AGTTCTATGGCCCAGACCCT-3', reverse primer 5'-TCTTTGAGATCCATGCCGT-3'; and interleukin-17 (IL-17): forward primer 5'-ACCGCAATGAAGACCCTGAT-3', reverse primer 5'-TCCCTCCGCATTGACACA-3'. The relative levels of mRNA expression were normalized to that of RPL32 (ribosomal protein L32, forward primer 5'-GAAACTGGCGGAAACCCA-3', reverse primer 5'-GGATCTGGCCCTTGAACCTT-3') mRNA. Non-reverse-transcribed RNA samples and water were included as negative controls.

Surgical destabilization of the medial meniscus (DMM) model in C57BL/6 mice

The *in vivo* protocols were accepted by the Geneva Authority (GE/170/14 and GE/99/15). DMM surgery was carried out on the right knee of 5-week-old male C57BL/6 mice (Charles Rivers, France) (n = 7 per group) (Fig. 3a). One week after surgery, 10 μ L of 2 % (w/v) NPPs were intra-articularly injected into the medial side on days 7 and 35 after the OA surgery as previously described [20] but with some modifications. In brief, after one week of acclimation, the mice were anesthetized using isoflurane, and a tracking chip (1.4 mm \times 8 mm) was inserted by subcutaneous (SC) dorsal injection. Under binocular microscopy (\times 10), a 5-mm longitudinal incision in the skin was performed on the right knee over the distal patella to the proximal medial tibial plateau using a # 11 blade. Then, the joint capsule was opened with a

longitudinal incision of 2 mm between the patellar ligament and the medial collateral ligament from the medial tibial plateau using an ultrafine micro-knife Sharpoint® with a 5-mm cutting edge (Fine Science Tools, Heidelberg, Germany). Finally, the meniscotibial ligament of the medial meniscus was sectioned, and the meniscus was displaced to confirm the destabilization. The suture line of the joint capsule was closed with one stitch of Vicryl® 4-0 suture, and the skin was closed with two stitches of Prolene® 5-0 suture (Ethicon, Somerville, MA, USA). One week post-surgery, NPPs suspended in PBS were injected *via* the IA route (day 7). The API doses of injected PH-NPPs and DXM-NPPs corresponded to 2.5, 2.01 mg·kg⁻¹, respectively. For the sham group, the ligament was only visualized by skin and joint capsule incisions (as described above) but was not transected or injected with PBS. On day 63, the total blood was collected for further analysis *via* intra-cardiac puncture under deep anesthesia, and the mice were sacrificed by spinal cord dislocation. The blood was added to tubes containing 1 mg of ethylenediaminetetraacetic acid dipotassium salt purchased from Sigma-Aldrich and directly centrifuged at 1,000 × *g* for 15 min and at 10,000 × *g* for 10 min at 4 °C. The plasma was collected and stored at -80 °C. The heart, kidneys, liver, spleen, and lungs were harvested, rinsed with NaCl 0.9 % and frozen at -20 °C.

Intravital fluorescence

Intravital fluorescence based on the Cy7 emission spectrum was assessed weekly in the mice using a Maestro M1 imaging system (Perkin Elmer, Cambridge

Research and Instrumentation Inc., Massachusetts) (acquisition settings: 650-950 in 10 nm steps, exposition time: 500 ms).

Histopathology and disease evaluation

5 Knee joints were collected and fixed in 4 % paraformaldehyde for 24 h. Whole joints were decalcified in 10 % (w/v) Tris-EDTA for 5 weeks on a shaker. The joints were embedded in paraffin, and 5 µm frontal (DMM) or sagittal (AIA) sections were taken at two levels of the joint at approximately 800 µm intervals. The slides were stained with H&E and toluidine blue for the AIA and OA model and further stained
10 with SOFG (safranin-O/fast green) for the DMM model. The disease severity of the AIA and OA models was assessed and scored by a pathologist (CAS) in a blinded manner.

 For the AIA model, semi-quantitative histological scores for synovial inflammation, neutrophil infiltration, cartilage and bone erosion were assessed by
15 grading from 0 to 4 as previously described [21].

 For the DMM model, cartilage thinning and cleft/cartilage erosion, bone erosion, and joint inflammation were evaluated using the following semi-quantitative scoring system: 0 (none), 1 (mild), 2 (moderate), 3 (severe). Furthermore, the overall osteoarthritic damage was evaluated using the published and recommended
20 Osteoarthritis Research Society International (OARSI) score [22] from 0 (normal) to 6 (very severe) as follows: 0 (normal), 0.5 (loss of safranin-O without structural changes), 1 (small fibrillations without loss of cartilage), 2 (vertical clefts down to the

layer immediately below the superficial layer and some loss of surface lamina), 3 (vertical clefts/erosion to the calcified cartilage extending to <25 % of the articular surface), 4 (vertical clefts/erosion to the calcified cartilage extending to 25-50 % of the articular surface), 5 (vertical clefts/erosion to the calcified cartilage extending to 50-75 % of the articular surface), and 6 (vertical clefts/erosion to the calcified cartilage extending to >75 % of the articular surface).

Fluorescence histology was also performed to analyze NPP distribution in the joints and adjacent tissues. Unstained paraffin-embedded joint tissue sections were analyzed by fluorescence microscopy (filter: DAPI and Cy7) on a Zeiss Axio Scan.Z1 scanner™ (Carl Zeiss, Jena, Germany).

Biodistribution study (DMM model)

The lungs, spleen, kidneys, heart, and liver from the sacrificed mice were ground for 60 seconds in 2-mL tubes containing 200 µL of acetonitrile and 6 metal beads (1/8") using a FASTPREP-24™ Instrument (MP Biomedicals, CA, Santa Ana, CA, USA) and then centrifuged at 10,000 × g for 20 min. Quantitative analysis of the supernatants containing drugs was performed using a Waters Acquity UPLC I-Class system (Waters, Milford, MA, USA) equipped with a binary solvent manager delivery pump and a sample manager autosampler with flow through a needle (SM-FTN). The chromatographic system was coupled to a Waters Xevo TQ-S triple quadrupole. Chromatographic separation was performed on a C18 Hypersil gold column (50/2.1, 1.9 µm bead particle size, Thermo Fisher Scientific). The mobile phase consisted of

0.1 % formic acid in water (A) and ACN (B). The optimized UHPLC elution conditions were 30–95 % A (0-4 min) and 95-30 % A (4–5 min) at a flow rate of 400 $\mu\text{L}\cdot\text{min}^{-1}$ with an injection volume of 10 μL . The Xevo TQ-S detector was exclusively operated in negative ESI mode. The optimal parameters for the high-sensitivity quantitation of PH and DXM were capillary 1 and 3 kV, cone 45 and 20 °, and collision 30 and 12, respectively and, for both, extractor 3 V. Data processing and peak integration were performed with TargetLynx software. The detection limits of PH and DXM were 1 and 10 ppb, respectively.

Micro-computed tomography (micro-CT) (DMM model)

Two months after the first IA injection, the mice were sacrificed, and their right knee joints were scanned using micro-CT (Quantum FX, PerkinElmer, Hopkinton, MA, USA) with a voxel size of 10 μm . The X-ray tube voltage was 90 kV, and the current was 88 μA . The software OsiriX MD Release 8.0 (OsiriX Foundation, Geneva, Switzerland) was used to measure the epiphysis thickness from the articular cartilage surface to the epiphyseal line at the center of the medial and lateral tibial epiphysis for all samples. All the samples were analyzed with a window level of 1500 and a window width of 3,000.

Multiplex enzyme-linked immunosorbent assay (ELISA) (DMM model)

Plasma samples from the mice were analyzed using a multiplex kit and beads purchased from Bio-Rad Laboratories, Inc. (Hercules, CA, USA) according to the

specifications of the manufacturer using the following OA biomarkers: IL-1 β , TNF α , and vascular endothelial growth factor (VEGF). Standard curves for each OA biomarker were generated using the reference cytokine concentration supplied by the manufacturers. The raw data were analyzed using the Bio-Plex Manager software
5 6.1 to obtain concentrations in $\mu\text{g}\cdot\text{mL}^{-1}$.

Statistical analysis

Data are expressed as the mean \pm standard deviation (s.d.). The statistical significance of the results was determined using Student's t-test (two groups), one-
10 way or two-way analysis of variance (ANOVA, multiple groups) and multiple comparisons (Tukey) in Prism 7.2 (GraphPad) with an alpha level of 0.05. The P values correspond to *P < 0.0332, **P < 0.0021, ***P < 0.0002, and ****P < 0.0001.

Results

Formulation and characterization of NPPs and MPs

PH and DXM nanocrystals were prepared in a two-step approach, i.e., (i) recrystallization and (ii) wet milling (Fig. 1a) [23]. The recrystallization process results
5 in a complete crystalline form of the starting material, and the wet milling process finally leads to the formation of nanocrystals. Various stabilizers were evaluated for their ability to produce small DXM crystals (Fig. 1b). The wet milling procedure was varied from 3 to 72 hours. Based on all experiments, TPGS, as a non-ionic surfactant, was selected for its high size reduction efficacy, its ability to suspend the nanocrystals
10 in aqueous media after their lyophilization/resuspension and its natural/non-toxic properties [24]. The final size of the PH and DXM nanocrystals after 6 h of wet milling ranged between 242 and 370 nm.

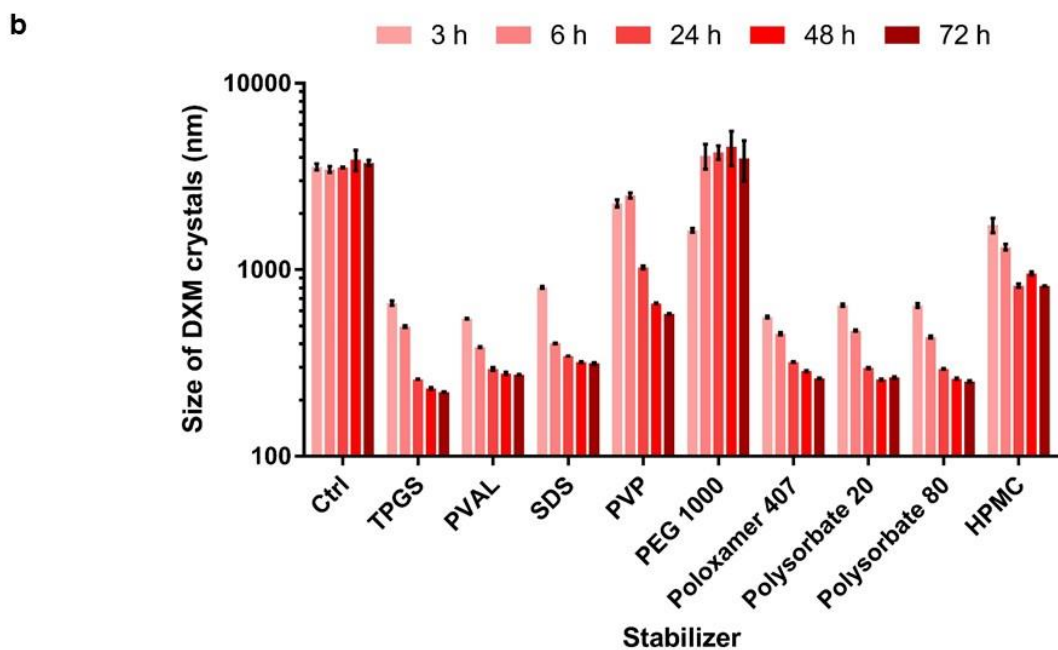
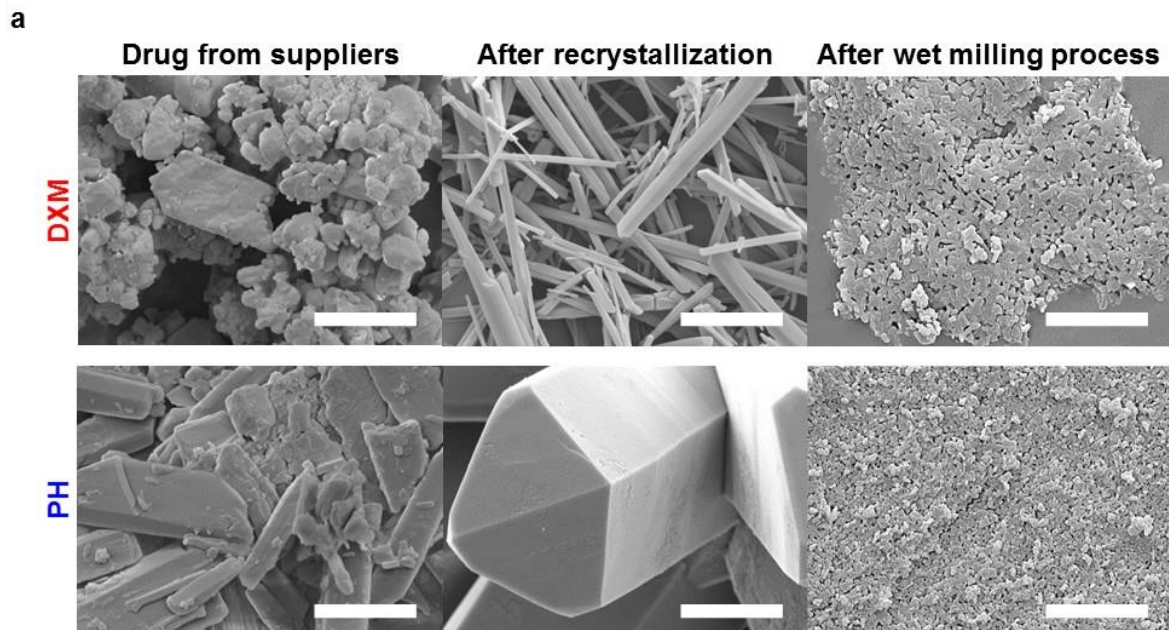
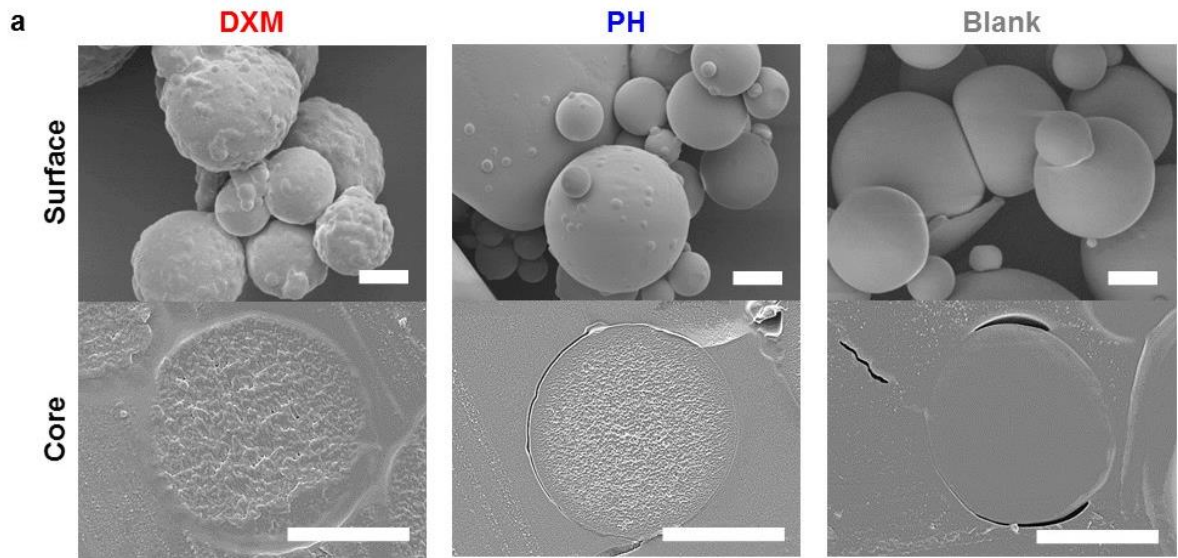


Figure 1 | Formulation of nanocrystals. **a**, Scanning electron micrographs of API crystals following the recrystallization process and wet milling process (at 6 h). Scale bar = 5 μm . **b**, Comparison between TPGS and various stabilizers used for the size reduction of DXM crystals in the wet milling process ($n = 3$, mean \pm s.d.). Ctrl: control without stabilizer, PVAL: poly(vinyl) alcohol, SDS: sodium dodecyl sulfate, PVP:

poly(vinyl pyrrolidinone), PEG: poly(ethylene glycol), HPMC: (hydroxypropyl)methyl cellulose.

In this study, a PLA covalently linked to Cyanine 7 (PLA-Cy7) was synthesized [17] as a biocompatible and biodegradable polymer for the intravital tracking of particles. A suspension of API nanocrystals in a solution of polymers (PLA-Cy7 at 0.1 % (w/w) in PLA) was spray-dried. Spherical NPPs were obtained (Fig. 2a). The rugosity of the cross sections indicated the presence of nanocrystals homogeneously distributed in the core of the particles, in contrast to the smooth surface of the blank NPPs (Fig. 2a; Fig. S1a,b,c). The endothermic events (T_m) determined by DSC confirmed the presence of crystalline forms of PH in the NPPs (Fig. S2). The melting point of PH in the PH-NPPs was shifted due to the presence of the polymer in the particles. The general characterization of PH-NPPs, DXM-NPPs, and blank NPPs is reported in Fig. 2b. No residual solvent was detected (below the detection limit of 0.5 ppb) in the final product by gas chromatography using the USP 467 method.

Additionally, the classical emulsification-evaporation method was used to formulate MPs composed of PLGA for a faster release of the drug (Fig. S3a,b,c). The characteristics of PH-MPs, DXM-MPs, and blank MPs are presented in Fig. 2b, showing an 8.5- to 10-fold increase in NPP drug loading compared to particles produced by the conventional methods for DXM and PH, respectively. Overall, sizes in the 10-15 μm range were considered to allow long-term joint retention without adverse effects [16]. All particles had negative zeta potentials ranging from -20 to -30 mV, enabling their facile re-dispersion in aqueous media.



b

Characterization	PH-NPPs	DXM-NPPs	Blank NPPs	PH-MPs	DXM-MPs	Blank MPs
Size Dv 0.5 (µm)	14.20	12.30	16.14	9.97	9.60	10.07
Span	2.42	2.37	2.65	1.85	1.62	2.47
% Drug loading	31.5	28.2	∅	3.1	3.3	∅
% Encapsulation	85.3	65.8	∅	95.9	98.9	∅
ζ-potential (mV)	-20.8	-23.9	-28.0	-32.0	-26.5	-27.7

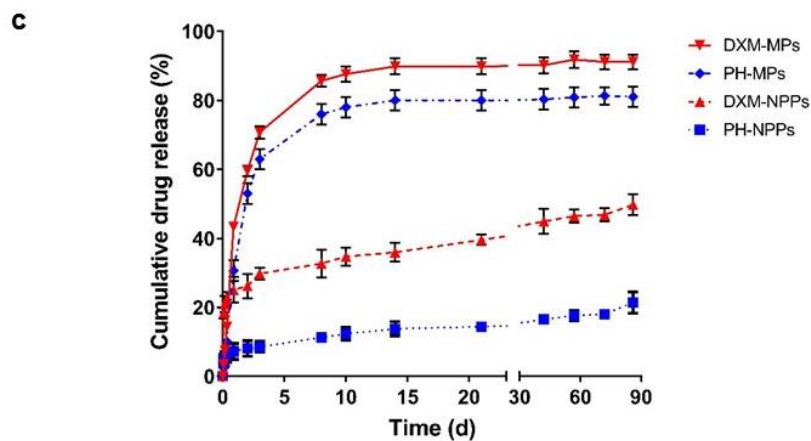


Figure 2 | Formulation and characterization of microparticles (NPPs and MPs).
a, Scanning electron micrographs of NPPs. Scale bar = 5 µm. **b**, Overview of NPP and MP characterization. **c**, Cumulative *in vitro* drug release profiles from MPs and NPPs over 3 months (n = 3, mean ± s.d.).

***In vitro* drug release profile and cell viability**

The four formulations, PH-NPPs, DXM-NPPs, PH-MPs, and DXM-MPs, presented different release kinetics *in vitro* (Fig. 2c). Drugs diffused out of the PH-MPs and DXM-MPs within 10-15 days (~80 % cumulative drug release). In contrast, 5 PH-NPPs and DXM-NPPs provided a prolonged drug release over at least 90 days with ~20-50 % cumulative drug release. A biphasic release profile was observed for NPPs as a burst phase in the first 3 days followed by a sustained near-zero-order kinetics release profile until day 90 (25.9 $\mu\text{g}\cdot\text{kg}^{-1}\cdot\text{week}^{-1}$ of PH: $r^2 = 0.89$ and 32.1 10 $\mu\text{g}\cdot\text{kg}^{-1}\cdot\text{week}^{-1}$ of DXM: $r^2 = 0.86$). The blank NPPs, PH-NPPs, and DXM-NPPs did not affect the cell viability of cultured OA human synoviocytes at a concentration 100-fold higher than IC_{50} values (Fig. S4 a,b,c).

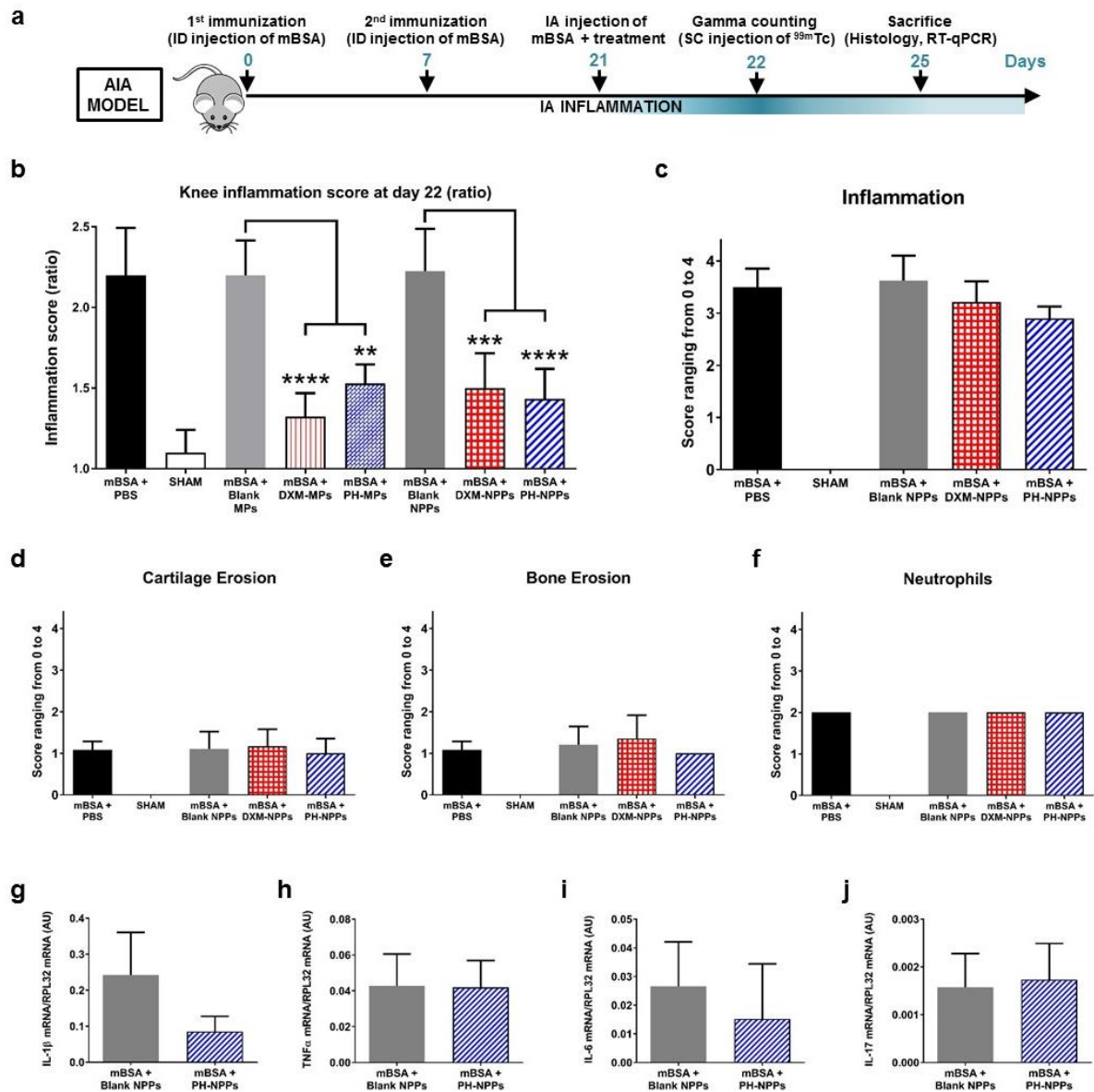


Figure 3 | AIA model, a short-term model of joint inflammation. ^{99m}Tc -uptake in affected joints on day 22 (b), histological assessment on day 25 (c-f), and cytokine analysis on day 25 (g-j) (n = 5-7 per group). a, General scheme of the *in vivo* experimental procedure of the AIA model. b, Knee inflammation assessed by ^{99m}Tc accumulation at day 22 (24 h post-IA injection). Histological scoring at day 25 (3 days post-IA injection) of c, inflammation, d, cartilage erosion e, bone erosion, and f, neutrophils. Quantification of mRNA levels of g, IL-1 β , h, TNF α , i, IL-6, and j, IL-17 in knee by RT-qPCR analysis. Data were normalized against the RPL32 housekeeping gene. *P < 0.0332, **P < 0.0021, *P < 0.0002, and ****P < 0.0001. All error bars represent the standard deviation from the mean.**

Analysis of *in vivo* efficacy in the AIA model (short-term model of joint inflammation)

Immunized mice were challenged with IA injection of an antigen (mBSA) as shown in Fig. 3a. The anti-inflammatory efficacy of NPPs and MPs was compared to that of non-active treatment controls, i.e., blank NPPs and blank MPs (polymer microparticles without drug) and a sham treatment condition (IA injection of PBS). All formulations were previously tested with a 29G insulin syringe to define the maximum injectable concentration of particles in PBS (force <5 N). The API doses of injected PH-NPPs, DXM-NPPs, and PH-MPs corresponded to the limit of injection 2, 2, and 45 % (w/v), respectively. The dose of injected DXM-MPs was selected to replicate a previous study [25]. Thus, the API doses of injected PH-NPPs, DXM-NPPs, PH-MPs, and DXM-MPs corresponded to 2.5, 2.01, 5, and 0.12 mg·kg⁻¹, respectively.

The inflammatory activity was assessed by ^{99m}Tc uptake (ratio) in the knee joints 24 h (day 22) after the IA injection of mBSA combined with treatment. The ^{99m}Tc accumulation ratio obtained for NPPs and MPs containing PH or DXM was significantly different from that obtained for the control animals treated with blank NPPs, blank MPs, and PBS (Fig. 3b). DXM and PH had a high anti-inflammatory effect. No statistically significant score differences were observed for blank NPPs and blank MPs compared to PBS alone, demonstrating that blank polymer microparticles did not induce higher ^{99m}Tc accumulation and inflammation by themselves.

Histological assessment of joint inflammation and destruction was also

performed on the NPP group after the sacrifice at 72 h post-mBSA challenge (day 25). The inflammation, as characterized by the presence of neutrophils and granulation tissue, was strong in intensity and reached the maximum score (4) (Fig. 3c). The inflammation score was numerically reduced for the PH-NPP group ($P = 0.0511$), almost achieving statistical significance compared to the DXM-NPP group ($P = 0.3895$). No difference between groups was observed in cartilage erosion (Fig. 3d), bone erosion (Fig. 3e) and neutrophils (Fig. 3f), which had mean scores of 1 (mild) and 2 (moderate), respectively.

The mRNA analysis of key pro-inflammatory cytokines in the knee joint, assessed by RT-qPCR of samples from the right knees of mice, revealed the effects of PH-NPPs on four different pro-inflammatory cytokines, IL-1 β , IL-6, IL-17, and TNF α (Fig. 3g,h,i,j). As shown in Fig. 3g, 4 days after the induction of arthritis, PH-NPP treatment reduced the mRNA expression of IL-1 β ($P = 0.0816$) in the arthritic joints compared to the use of blank NPPs. In addition, PH-NPPs tended to decrease the IL-6 mRNA level (Fig. 3i) ($P = 0.3914$), but no evidence of PH activity on mRNA TNF α and IL-17 was observed.

The IA persistence of NPPs and MPs was demonstrated at day 25 (4 days after injection) on histological slides using light microscopy. The semi-quantitative intravital analysis of Cy7 fluorescence (NPPs) monitored for 4 days and the fluorescence microscopy of histological slides also supported particle persistence in the joints.

After the first screening of the anti-inflammatory activity of NPPs or MPs loaded

with PH and DXM in the AIA model (short-term inflammatory model), we shifted to a long-term DMM model presenting all characteristics of OA in humans with slow disease progression and moderate severity.

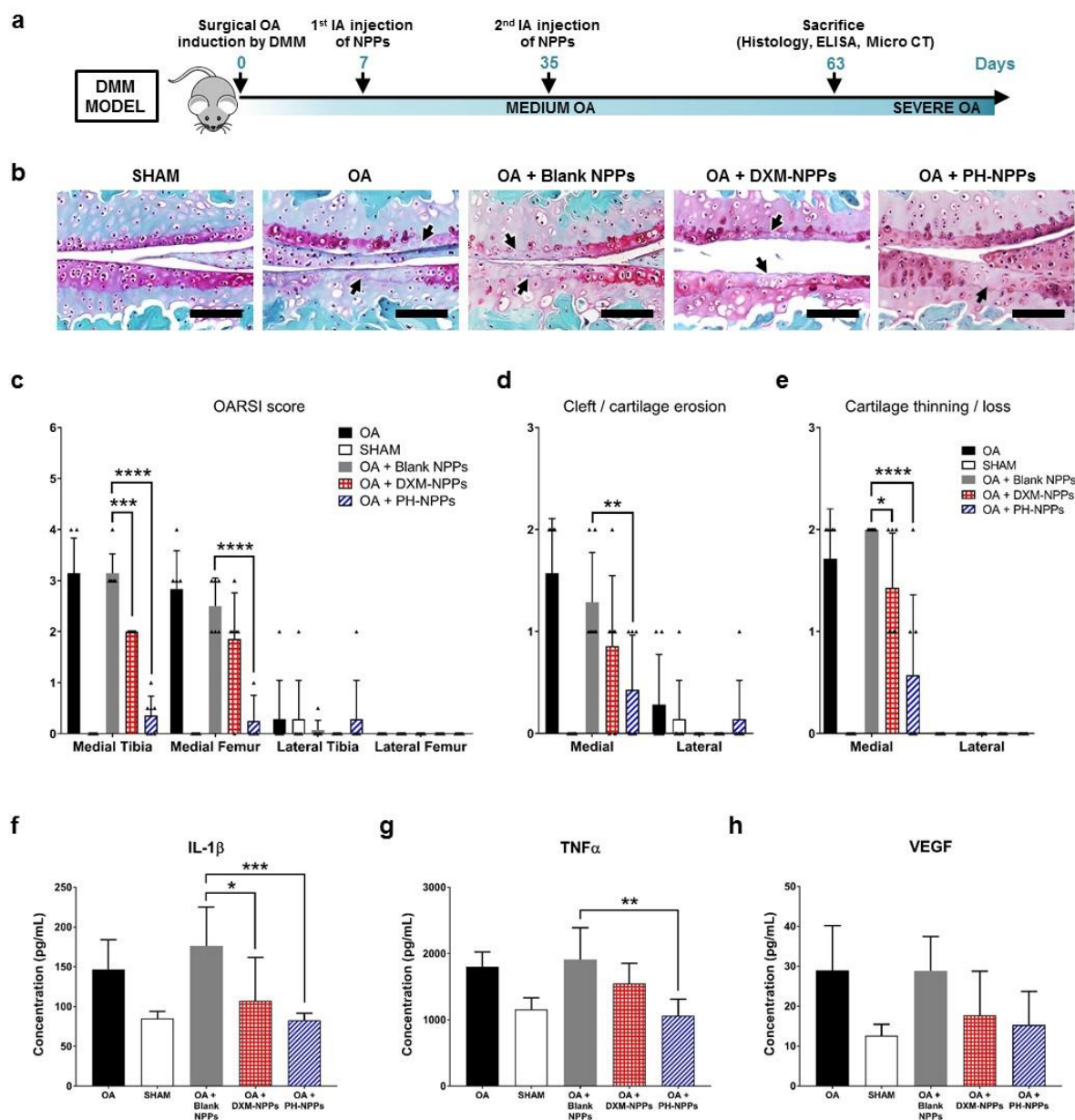


Figure 4 | DMM model, a long-term model of OA. Histological assessment of disease activity and multiplex ELISA analysis of plasma inflammatory cytokines (n = 7 per group). **a**, General scheme of the *in vivo* experimental procedure of the DMM model. **b**, Representative SOFG photomicrographs showing the medial side of mouse knees at 63 days. Femur (above), tibial (below), cartilage stain in purple. Arrows indicate OA damage. Scale bar = 100 μ m. Histological scoring of **c**, OARSI score from 0 to 6, **d**, cleft/cartilage erosion, and **e**, cartilage thinning/loss scores from 0 to 3. Multiplex ELISA analysis of **f**, IL-1 β , **g**, TNF α , and **h**, VEGF in plasma from mice at 63 days. *P < 0.0332, **P < 0.0021, ***P < 0.0002, and ****P < 0.0001. All error bars represent the standard deviation from the mean.

Analysis of *in vivo* efficacy in the long-term mechanistic DMM OA model

PH-NPPs and DXM-NPPs were selected for having long-term *in vitro* release properties for a chronic disease model. For these experiments, we selected a murine mechanical model based on surgical DMM. This model affects the meniscus, which is commonly involved in human OA [20]. In the right knees of mice, the medial meniscotibial ligament was sectioned at day 0, and two IA injections were administered at days 7 and 35 in the medial part of the destabilized knee (Fig. 4a). The doses of PH and DXM administered were similar to those in the AIA model (2.5 and 2.01 mg·kg⁻¹, respectively). The biodistribution study showed no PH or DXM above the detection limits in the liver, lungs, spleen, kidneys, and heart, according to UHPLC-MS/MS. Mouse weight monitoring did not reveal any significant difference between the OA and sham groups several weeks after surgery, supporting the non-debilitating nature of the surgical procedure (Fig. S5).

As shown in Fig. 4b, representative histological samples of joint sections present cartilage damage located on the medial half of the knee joint in the groups

affected by OA (lateral half used as an internal control). No disease activity was observed in the sham group (negative control). Two months after the destabilization, the maximum OARSI score in the OA control group was 4 (mean value = 3), corresponding to moderate severity in this OA model. In addition, the medial tibia correlates positively and closely with the medial femur OARSI scoring ($r^2 = 0.905$). No treatment effect of blank NPPs (control formulations) was found compared to the OA group. In the medial tibial cartilage, PH-NPPs and DXM-NPPs showed a significantly different OARSI score from that of the OA group (Fig. 4c). A loss of safranin-O without structural changes for PH-NPPs, vertical clefts down to the layer immediately below the superficial layer and some loss of surface lamina for DXM-NPPs were the main observations. Only PH-NPPs resulted in a cleft/cartilage erosion scoring reduction ($P = 0.0033$) compared to blank NPPs (Fig. 4d). The bioactivity of PH-NPPs ($P = <0.0001$) and DXM-NPPs ($P = 0.0243$) significantly reduced cartilage thinning/loss (Fig. 4e).

At day 63, immediately before sacrifice, a cardiac puncture was performed to withdraw blood for quantifying the expression of 3 biomarkers in the total plasma. The down-regulation of the expression of IL-1 β ($P = 0.0002$) and TNF α ($P = 0.005$), and the downward trend of VEGF ($P = 0.0946$) demonstrated the *in vivo* efficacy of the PH-NPP treatment (Fig. 4f,g,h). As already shown in Fig. 3g, PH reduced the mRNA level of pro-inflammatory cytokine IL-1 β [25]. In contrast, the DXM-NPP treatment was less effective and inhibited only IL-1 β mRNA expression in plasma ($P = 0.0459$) (Fig. 4f).

Much as in the AIA model, the persistence of NPPs was monitored by intravital fluorescence imaging in the DMM model. After two months, NPPs with a mean diameter of 10-15 micrometers were effectively retained in the joint and the adjacent tissues (Fig. S6). NPPs were mainly present in the articular soft tissues, either in the extracellular space, demarcated by foamy macrophages and some giant cells, or intracellularly within foamy macrophages. At the time of sacrifice, no strong tissue inflammation was seen overall. Finally, micro-CT imaging revealed an increased medial tibial epiphysis density on the axial plane slices of groups affected by OA compared to the sham group (Fig. S7a). No differences between the treatment and control groups were detected in the percentage ratio of medial to lateral tibial epiphysis thickness by micro-CT (Fig. S7b) or in bone erosion by histological analysis.

Discussion

The existing pharmacopeia lacks efficient APIs to treat and slow down the progression of OA. PH appears to be a promising p38 α / β MAPK inhibitor that partly fills these gaps. However, the effect of PH after oral administration was not sustained after two weeks in patients with RA [1], and the results of a phase 2 clinical trial in OA patients are not yet available. It is attractive to consider the local administration of PH in order to increase IA concentrations and lower the systemic exposure and associated systemic adverse effects. The aim of this study was to explore the potential utility of biodegradable NPPs loaded with a sufficiently high amount of PH,

a p38 α/β MAPK inhibitor, to enable the IA release of API at therapeutic doses over several months. *In vivo* efficacy studies were performed in two different mouse models ((i) a short-term inflammatory AIA model and (ii) a long-term non-inflammatory mechanistic DMM OA model) to demonstrate the clinical efficacy of PH-loaded particles. DXM, a classical steroid, was used as a reference API.

Previously, our group has shown that the IA administration of 10- μ m microparticles resulted in prolonged local articular soft tissue retention and did not lead to a relevant inflammatory response [16]. The approach taken in this study is a new drug-carrier system, namely, NPPs. To significantly reduce the burst and to prolong the release of PH over months, we formulated nanocrystals [3, 4] by a wet milling process [24, 26]. TPGS proved to be an efficient stabilizer for PH. For the biodegradable polymer matrix, we selected PLA and PLGA, since MPs of these polymers do not lead to synovial inflammation after IA injection [5, 6]. We selected PLGA (75:25) to formulate PH-loaded MPs. PLA was chosen for NPPs in order to firmly embed the nanocrystals of PH and provide long-term drug release for formulations intended to remain for months in the articular soft tissues. Additionally, we added to the composition of the NPPs a small percentage of PLA covalently tagged with Cy7, thus enabling intravital monitoring of the MPs [7]. PH-NPPs and DXM-NPPs were obtained by spray-drying nanocrystals suspended in a polymer solution. The NPPs were compared with PH-MPs and DXM-MPs formulated by the conventional emulsification-evaporation method. Embedding nanocrystals in MPs by spray drying produced up to a 10-fold increase in drug loading compared to the usual

emulsification-diffusion process. The process of formulation by spray drying is fast, and the organic solvent is very rapidly evaporated [8]. Additionally, spray drying is a robust method for scaling up. In this study, this process hindered the dissolution of API nanocrystals and led to very high drug loadings inside the PLA matrix. *In vitro* release trials revealed that for both PH and DXM, the NPP formulations reduced the burst significantly and provided a near-zero-order kinetic profile for weeks in line with the features required for an IA OA treatment. Embedding nanocrystals of API in a polymer matrix rather than having API in the matrix dramatically changed the release profile. The *in vitro* release rate from NPPs and MPs at 24 h suggests that this method of administration makes the drug available with a therapeutic effect.

To assess the functional relevance and potential clinical efficacy of PH delivered IA in the short term (up to 3 days), PH-NPPs and PH-MPs were tested in the inflammatory AIA model. The administration of NPPs, although featuring a minute daily drug release (Fig. 2c), provided relevant bioactivity comparable to that of MPs over the first hours and days following injection. The release of PH- or DXM-NPPs after one injection was sufficient to induce a pharmacological treatment response, as observed by the reduction in the ^{99m}Tc uptake and by the histological grade of the inflammation. RT-qPCR assays performed on tissues collected four days after the initiation of IA treatment revealed a numerical reduction in IL-6 and IL-1 β mRNA expression, but the reduction did not achieve statistical significance. Indeed, in a murine AIA model, the mRNA levels of cytokines decreased from day 22 to day 25 [27].

The fact that NPPs contained 8-10-fold more drug than conventional MPs and their sustained release profile encouraged long-term *in vivo* experiments. Following the positive short-term results of the AIA model, we shifted to a relevant long-term OA murine model [28] based on surgical DMM to validate the *in vivo* efficacy of PH-NPPs toward cartilage over two months. The local sustained release of a high API dose provided by the PH-NPPs enabled effective cartilage protection, maintaining an active drug concentration despite the expected rapid joint clearance [4]. This protective effect might be partly explained by a reduced apoptotic rate of chondrocytes under p38 inhibition through p-ATF-2 down-regulation [29]. In contrast, DXM-NPPs showed a lower efficiency of this effect, as shown by the histology scoring results (Fig. 4c,d,e). Multiplex ELISA was used to quantify OA biomarkers in mouse plasma at day 63. Compared to the DXM-NPPs, PH-NPP treatment led to a more significant reduction in the mRNA expression levels of inflammatory cytokines such as IL-1 β and TNF α in plasma (Fig. 4f,g). These results substantiate the ability of the PH-NPPs to relieve inflammation processes in the long term. The histological analysis of the knees did not show any histological abnormalities or signs of inflammation or synovial hyperplasia, which confirms good compatibility between the NPPs and the synovial tissues. This result and that of a cell viability assay on human fibroblast-like synoviocytes further support this line of evidence. No effects of the treatments were observed in the thickness ratio of the epiphysis (rounded end of the tibia) measured from 3D X-ray microtomographs. The biodistribution study performed in various organs at day 63 confirmed the limited systemic exposure to PH (<0.5 ng·mL⁻¹) and

the local tissue persistence of PH-NPPs. In comparison, the human plasma concentration for orally administered PH (30 mg) was reported to be 49.2 ng·mL⁻¹ at 30.5 h [9].

Taken together, our data show that PH-NPPs fulfill important needs for the treatment of OA such as (i) long-term joint retention, (ii) good biocompatibility, and (iii) high drug loading with controlled and extended release over months. The short-term AIA study in mice revealed the bioactivity of locally injected PH, even using PH-NPPs designed to release the API over months. The lack of bioactivity at day 25 might be related to the model itself, specifically the development of acute inflammation.

Using the mechanistic long-term DMM model, with slow and progressive cartilage damage, it was possible to demonstrate significantly superior bioactivity of PH-NPPs over two months. The IA retention monitored by intravital imaging, the cytokine expression, and the OARSI scores validated the *in vivo* efficacy. In this study, we demonstrated that the local administration of PH combined with technology enabling near-zero-order kinetics is crucial to show utility in a mechanistic murine OA model while limiting the risk of systemic toxicity. For future experiments, testing the PH-NPPs in a chronic model in large animals should be considered to confirm the present *in vivo* proof of concept and further substantiate the potential usefulness of this treatment approach for human OA.

Conclusions

A local drug delivery system adapted for the treatment of OA was successfully developed. Nanocrystals of PH and DXM were optimized, stabilized and dispersed in a PLA matrix, forming PH-NPPs and DXM-NPPs. Compared to the conventional MPs formulated with PLGA, NPPs encapsulated up to 10-fold more API and displayed an ideal near-zero-order release profile *in vitro*. No *in vitro* toxicity to cultured OA synoviocytes was observed. The short-term AIA model was useful as an *in vivo* proof of concept of PH-NPP-dependent inflammation reduction. The mechanistic long-term DMM model, as a chronic disease model relevant to human OA, confirmed the ability of PH-NPPs to slow down cartilage degradation/degeneration and to lower pro-inflammatory cytokine levels more efficiently than DXM-NPPs. All in all, the PH-NPPs shown an ideal effect, slowing down OA progression due to a slight burst release in the first days followed by a prolonged release over months. PH-NPPs should be tested in larger OA animal models, such as sheep, to provide additional evidence supporting this approach as a relevant treatment option for human OA.

Supplementary material

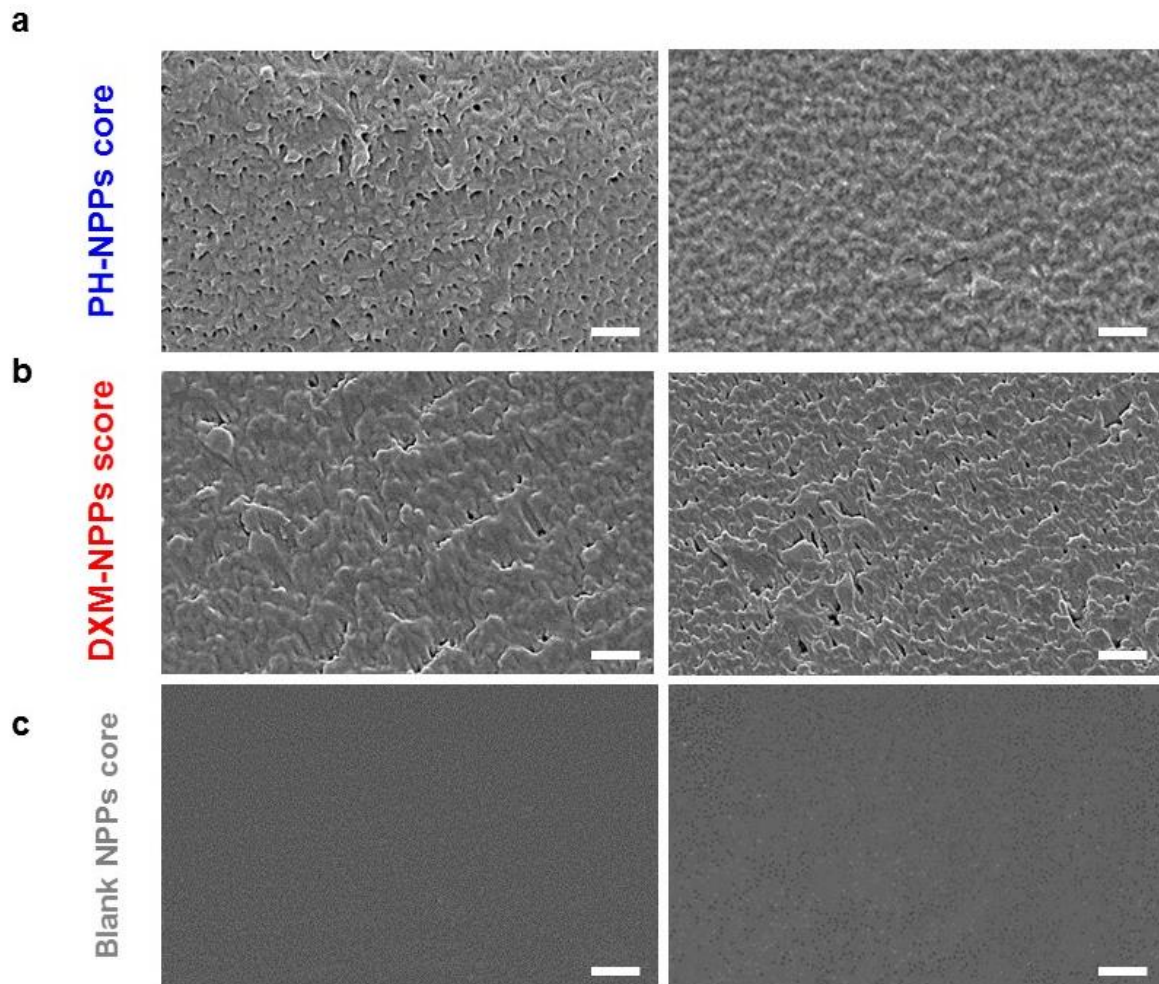


Figure S1 | Scanning electron micrographs of **a**, PH-NPPs, **b**, DXM-NPPs and **c**, blank NPPs core. Scale bar = 1 μm .

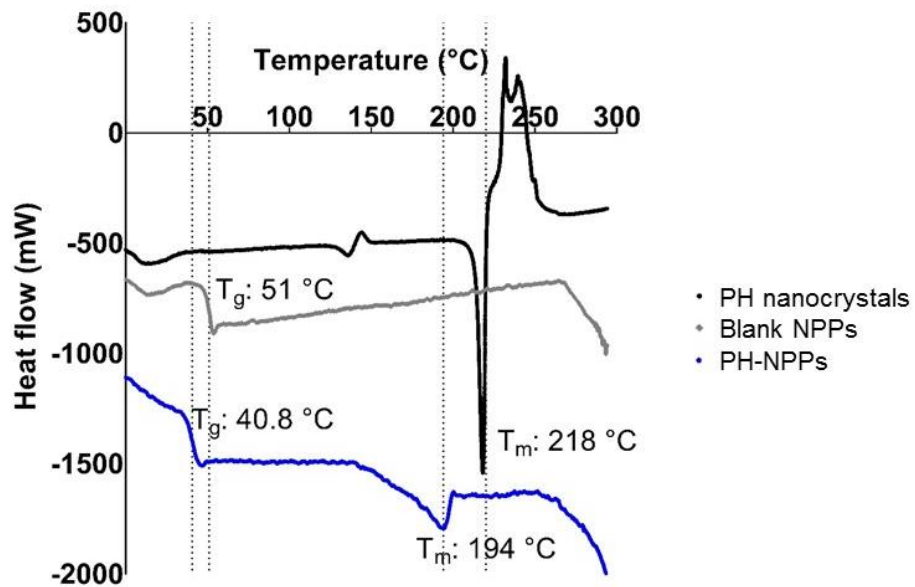


Figure S2 | Differential scanning calorimetry thermographs of PH nanocrystals and PH-NPPs compared to blank NPPs. T_g: glass transition temperature (polymer), T_m: melting temperature (endothermic event).

5

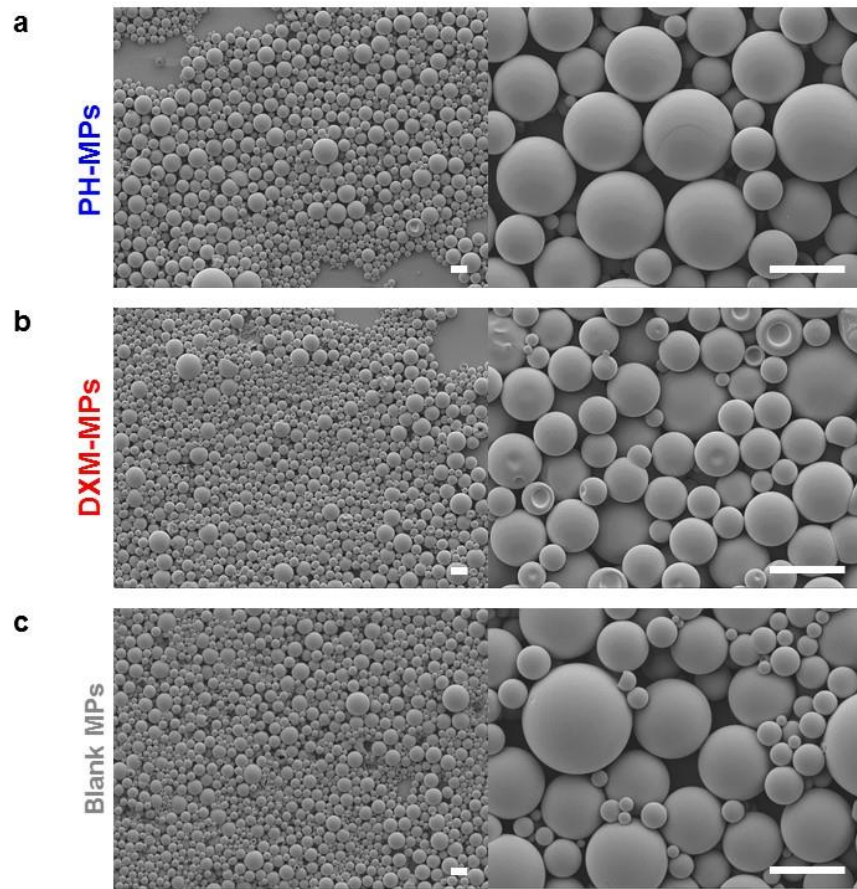


Figure S3 | Scanning electron micrographs of **a**, PH-MPs, **b**, DXM-MPs and **c**, blank MPs. Scale bar = 10 μm .

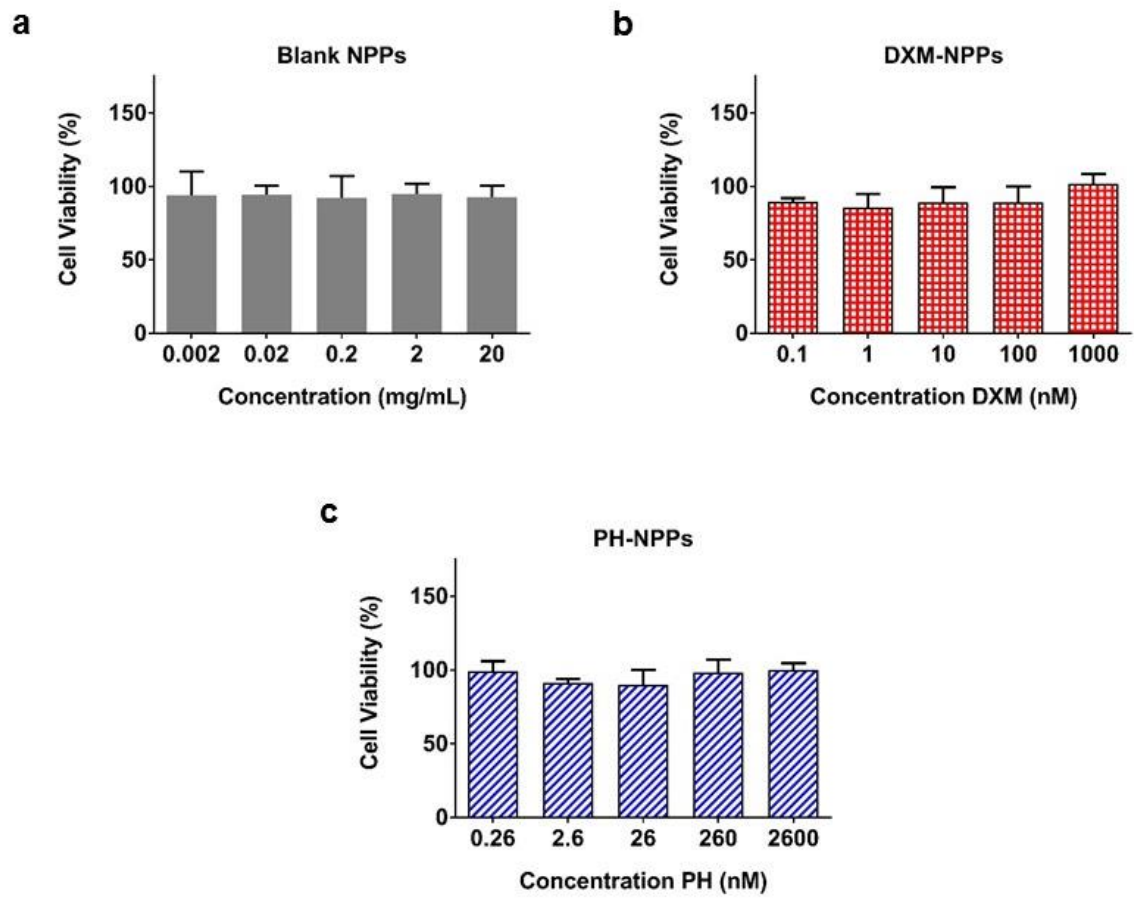


Figure S4 | Mitochondrial activity of human fibroblast-like synoviocytes exposed to **a**, blank NPPs **b**, DXM-NPPs and **c**, PH-NPPs (mean \pm s.d.).

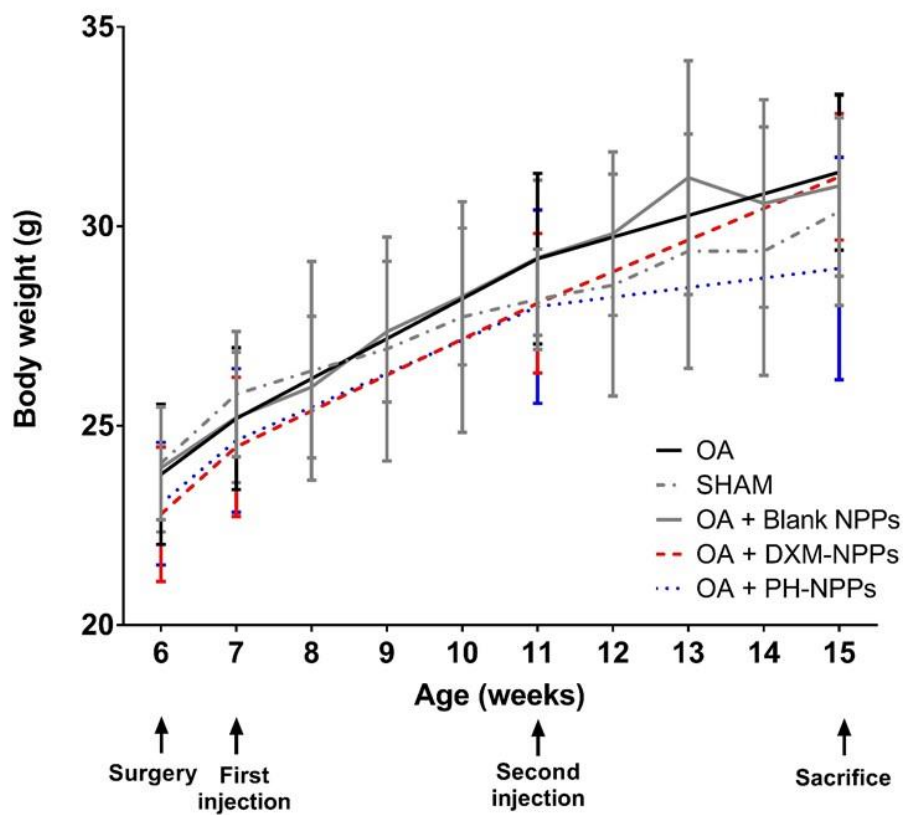


Figure S5 | Body weight curves of male mice C57BL/6J as a function of age in weeks from the surgery to the sacrifice (mean \pm s.d.).

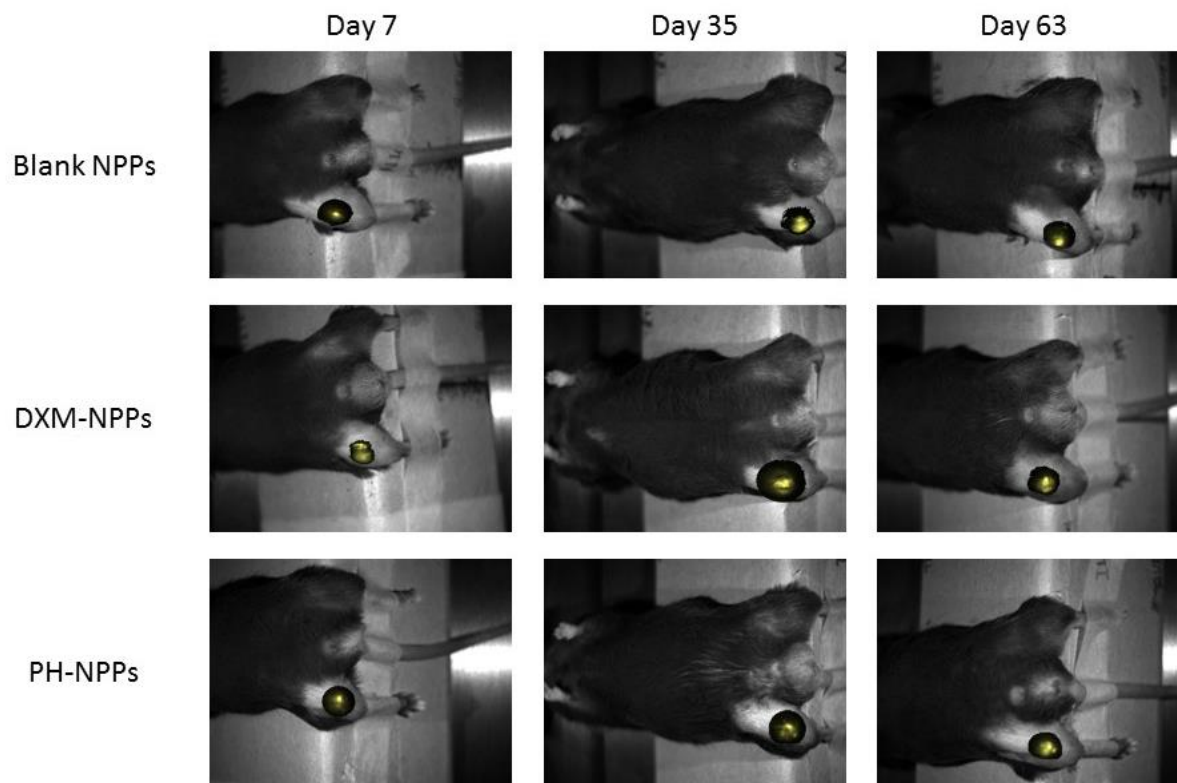


Figure S6 | Representative photographs of intravital fluorescence of NPPs (yellow) superimposed on white light images of mice up to 63 days in DMM mouse model (n = 7, injection volume: 10 μ L).

5

10

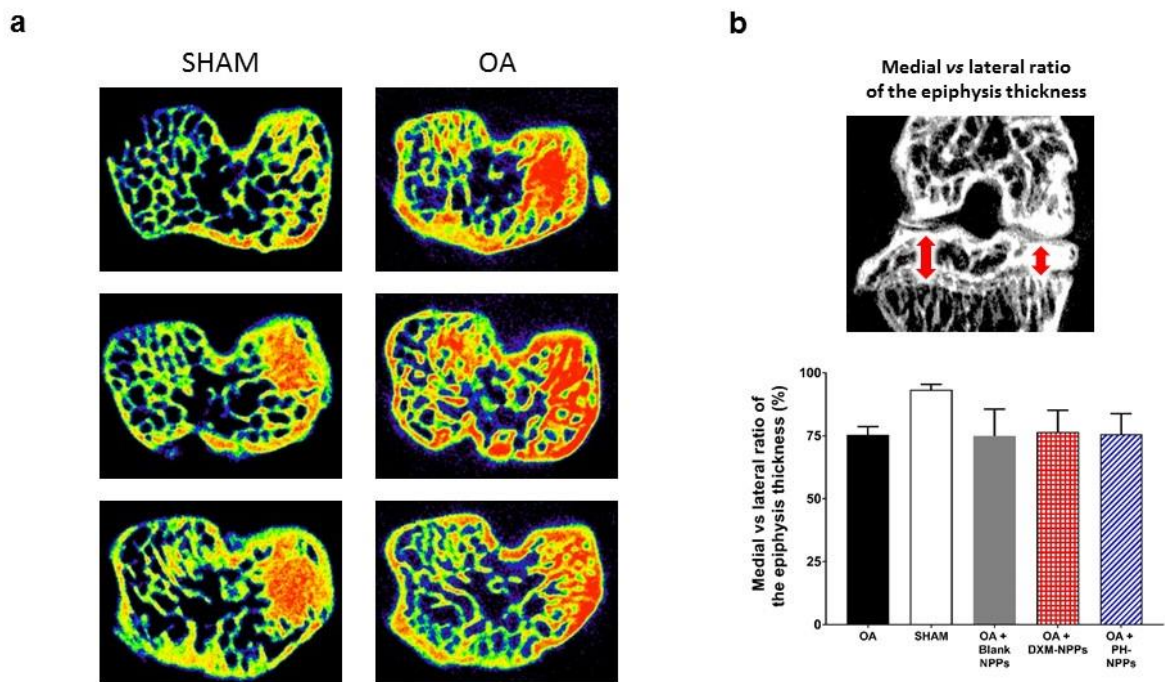


Figure S7 | Micro-CT bone analysis. **a**, Axial plane of 3 representative micro-CT slices of the tibial epiphysis of the OA and sham groups at day 63 (left: lateral, right: medial). Fluorescence scale from blue (low bone density) to red (high bone density). Identical image processing. **b**, Percentage of medial to lateral tibial epiphysis thickness (mean \pm s.d.).

References

- [1] Osteoarthritis, in, WHO Department of Chronic Diseases and Health Promotion, www.who.int/medicines/areas/priority_medicines/Ch6_12Osteo.pdf [Accessed 8/14/17].
- [2] J. Martel-Pelletier, A.J. Barr, F.M. Cicuttini, P.G. Conaghan, C. Cooper, M.B. Goldring, S.R. Goldring, G. Jones, A.J. Teichtahl, J.P. Pelletier, Osteoarthritis, *Nat Rev Dis Primers*, 2 (2016) 16072.
- [3] A.S. Lee, M.B. Ellman, D. Yan, J.S. Kroin, B.J. Cole, A.J. van Wijnen, H.-J. Im, A current review of molecular mechanisms regarding osteoarthritis and pain, *Gene*, 527 (2013) 440-447.
- [4] C.H. Evans, V.B. Kraus, L.A. Setton, Progress in intra-articular therapy, *Nat. Rev. Rheumatol.*, 10 (2014) 11-22.
- [5] X. Yang, H. Du, G. Zhai, Progress in Intra-Articular Drug Delivery Systems for Osteoarthritis, *Curr. Drug Targets*, 15 (2014) 888-900.
- [6] H.R. Hope, G.D. Anderson, B.L. Burnette, R.P. Compton, R.V. Devraj, J.L. Hirsch, R.H. Keith, X. Li, G. Mbalaviele, D.M. Messing, M.J. Saabye, J.F. Schindler, S.R. Selness, L.I. Stillwell, E.G. Webb, J. Zhang, J.B. Monahan, Anti-Inflammatory Properties of a Novel N-Phenyl Pyridinone Inhibitor of p38 Mitogen-Activated Protein Kinase: Preclinical-to-Clinical Translation, *Journal of Pharmacology and Experimental Therapeutics*, 331 (2009) 882-895.
- [7] L. Xing, H.S. Shieh, S.R. Selness, R.V. Devraj, J.K. Walker, B. Devadas, H.R. Hope, R.P. Compton, J.F. Schindler, J.L. Hirsch, A.G. Benson, R.G. Kurumbail, R.A. Stegeman, J.M. Williams, R.M. Broadus, Z. Walden, J.B. Monahan, Structural Bioinformatics-Based Prediction of Exceptional Selectivity of p38 MAP Kinase Inhibitor PH-797804, *Biochemistry*, 48 (2009) 6402-6411.
- [8] S.R. Selness, R.V. Devraj, B. Devadas, J.K. Walker, T.L. Boehm, R.C. Durley, H. Shieh, L. Xing, P.V. Rucker, K.D. Jerome, A.G. Benson, L.D. Marrufo, H.M. Madsen, J. Hitchcock, T.J. Owen, L. Christie, M.A. Promo, B.S. Hickory, E. Alvira, W. Naing, R. Bleviss-Bal, D. Messing, J. Yang, M.K. Mao, G. Yalamanchili, R.V. Embse, J. Hirsch, M. Saabye, S. Bonar, E. Webb, G. Anderson, J.B. Monahan, Discovery of PH-797804, a highly selective and potent inhibitor of p38 MAP kinase, *Bioorg Med Chem Lett*, 21 (2011) 4066-4071.
- [9] D. Singh, L. Siew, J. Christensen, J. Plumb, G.W. Clarke, S. Greenaway, C. Perros-Huguet, N. Clarke, I. Kilty, L. Tan, Oral and inhaled p38 MAPK inhibitors: effects on inhaled LPS challenge in healthy subjects, *Eur J Clin Pharmacol*, 71 (2015) 1175-1184.
- [10] J. Pradal, M.-F. Zuluaga, P. Maudens, J.-M. Waldburger, C.A. Seemayer, E. Doelker, C. Gabay, O. Jordan, E. Allémann, Intra-articular bioactivity of a p38 MAPK inhibitor and development of an extended-release system, *Eur. J. Pharm. Biopharm.*, 93 (2015) 110-117.
- [11] I. Prasadam, X. Mao, Y. Wang, W. Shi, R. Crawford, Y. Xiao, Inhibition of p38 pathway leads to OA-like changes in a rat animal model, *Rheumatology (Oxford)*, 51 (2012) 813-823.
- [12] H.Y. Yong, M.S. Koh, A. Moon, The p38 MAPK inhibitors for the treatment of inflammatory diseases and cancer, *Expert Opin Investig Drugs*, 18 (2009) 1893-1905.
- [13] L. Xing, Clinical candidates of small molecule p38 MAPK inhibitors for inflammatory diseases, 2016, 4 (2016).

- [14] M. Janssen, G. Mihov, T. Welting, J. Thies, P. Emans, Drugs and polymers for delivery systems in OA joints: clinical needs and opportunities, *Polymers (Basel, Switz.)*, 6 (2014) 799-819, 721 pp.
- [15] N. Butoescu, O. Jordan, E. Doelker, Intra-articular drug delivery systems for the treatment of rheumatic diseases: A review of the factors influencing their performance, *European Journal of Pharmaceutics and Biopharmaceutics*, 73 (2009) 205-218.
- [16] J. Pradal, P. Maudens, C. Gabay, C.A. Seemayer, O. Jordan, E. Allémann, Effect of particle size on the biodistribution of nano- and microparticles following intra-articular injection in mice, *Int. J. Pharm.*, 498 (2016) 119-129.
- [17] P. Maudens, C.A. Seemayer, C. Thauvin, C. Gabay, O. Jordan, E. Allemann, Nanocrystal-Polymer Particles: Extended Delivery Carriers for Osteoarthritis Treatment, *Small*, (2018).
- [18] D. Brackertz, G.F. Mitchell, M.A. Vadas, I.R. Mackay, Studies on antigen-induced arthritis in mice. III. Cell and serum transfer experiments, *J Immunol*, 118 (1977) 1645-1648.
- [19] D. Brackertz, G.F. Mitchell, M.A. Vadas, I.R. Mackay, J.F. Miller, Studies on antigen-induced arthritis in mice. II. Immunologic correlates of arthritis susceptibility in mice, *J Immunol*, 118 (1977) 1639-1644.
- [20] S.S. Glasson, T.J. Blanchet, E.A. Morris, The surgical destabilization of the medial meniscus (DMM) model of osteoarthritis in the 129/SvEv mouse, *Osteoarthritis Cartilage*, 15 (2007) 1061-1069.
- [21] P. Martin, D. Talabot-Ayer, C.A. Seemayer, S. Vigne, C. Lamacchia, E. Rodriguez, A. Finckh, D.E. Smith, C. Gabay, G. Palmer, Disease severity in K/BxN serum transfer-induced arthritis is not affected by IL-33 deficiency, *Arthritis Research & Therapy*, 15 (2013) R13-R13.
- [22] S.S. Glasson, M.G. Chambers, W.B. Van Den Berg, C.B. Little, The OARSI histopathology initiative - recommendations for histological assessments of osteoarthritis in the mouse, *Osteoarthritis Cartilage*, 18 Suppl 3 (2010) S17-23.
- [23] S. Dorsaz, T. Snaka, Q. Favre-Godal, P. Maudens, N. Boulens, P. Furrer, S.N. Ebrahimi, M. Hamburger, E. Allémann, K. Gindro, E.F. Queiroz, H. Riezman, J.-L. Wolfender, D. Sanglard, Identification and mode of action of a plant natural product targeting human fungal pathogens, *Antimicrob Agents Chemother*, (2017).
- [24] Y. Guo, J. Luo, S. Tan, B.O. Otieno, Z. Zhang, The applications of Vitamin E TPGS in drug delivery, *Eur. J. Pharm. Sci.*, 49 (2013) 175-186.
- [25] N. Butoescu, C.A. Seemayer, G. Palmer, P.-A. Guerne, C. Gabay, E. Doelker, O. Jordan, Magnetically retainable microparticles for drug delivery to the joint: efficacy studies in an antigen-induced arthritis model in mice, *Arthritis Res. Ther.*, 11 (2009) No pp. given.
- [26] Y. Liu, L. Huang, F. Liu, Paclitaxel nanocrystals for overcoming multidrug resistance in cancer, *Mol. Pharm.*, 7 (2010) 863-869.
- [27] D. Pohlers, A. Siegling, E. Buchner, C.B. Schmidt-Weber, E. Palombo-Kinne, F. Emmrich, R. Brauer, R.W. Kinne, Expression of cytokine mRNA and protein in joints and lymphoid organs during the course of rat antigen-induced arthritis, *Arthritis Res Ther*, 7 (2005) R445-457.

[28] C.B. Little, S. Zaki, What constitutes an “animal model of osteoarthritis” – the need for consensus?, *Osteoarthritis and Cartilage*, 20 (2012) 261-267.

[29] J. Han, X. Guo, W. Tan, F. Zhang, J. Liu, W. Wang, P. Xu, M.J. Lammi, The expression of p-ATF2 involved in the chondrocytes apoptosis of an endemic osteoarthritis, Kashin-Beck disease, *BMC Musculoskeletal Disorders*, 14 (2013) 209.

5